JOURNAL OF BACTERIOLOGY, July 2010, p. 3368–3378 Vol. 192, No. 13
0021-9193/10/$12.00 doi:10.1128/JB.01371-09

Mutations in the Lipopolysaccharide Biosynthesis Pathway Interfere with Crescentin-Mediated Cell Curvature in *Caulobacter crescentus*▽§

Matthew T. Cabeen,[1]‡ Michelle A. Murolo,[1]‡† Ariane Briegel,[2,5] N. Khai Bui,[3] Waldemar Vollmer,[3] Nora Ausmees,[4] Grant J. Jensen,[2,5] and Christine Jacobs-Wagner[1,6,7]*

Department of Molecular, Cellular and Developmental Biology, Yale University, New Haven, Connecticut 06520[1]; Division of Biology, California Institute of Technology, 1200 E. California Blvd., Pasadena, California 91125[2]; Centre for Bacterial Cell Biology, Institute for Cell and Molecular Biosciences, Newcastle University, Richardson Road, Newcastle upon Tyne NE2 4AX, United Kingdom[3]; Department of Cell and Molecular Biology, Uppsala University, BMC Box 596, 75124 Uppsala, Sweden[4]; Howard Hughes Medical Institute, California Institute of Technology, Pasadena, California 91125[5]; Section of Microbial Pathogenesis, Yale School of Medicine, New Haven, Connecticut 06510[6]; and Howard Hughes Medical Institute, Yale University, New Haven, Connecticut 06520[7]

Received 19 October 2009/Accepted 20 April 2010

Bacterial cell morphogenesis requires coordination among multiple cellular systems, including the bacterial cytoskeleton and the cell wall. In the vibrioid bacterium *Caulobacter crescentus*, the intermediate filament-like protein crescentin forms a cell envelope-associated cytoskeletal structure that controls cell wall growth to generate cell curvature. We undertook a genetic screen to find other cellular components important for cell curvature. Here we report that deletion of a gene (*wbqL*) involved in the lipopolysaccharide (LPS) biosynthesis pathway abolishes cell curvature. Loss of WbqL function leads to the accumulation of an aberrant O-polysaccharide species and to the release of the S layer in the culture medium. Epistasis and microscopy experiments show that neither S-layer nor O-polysaccharide production is required for curved cell morphology *per se* but that production of the altered O-polysaccharide species abolishes cell curvature by apparently interfering with the ability of the crescentin structure to associate with the cell envelope. Our data suggest that perturbations in a cellular pathway that is itself fully dispensable for cell curvature can cause a disruption of cell morphogenesis, highlighting the delicate harmony among unrelated cellular systems. Using the *wbqL* mutant, we also show that the normal assembly and growth properties of the crescentin structure are independent of its association with the cell envelope. However, this envelope association is important for facilitating the local disruption of the stable crescentin structure at the division site during cytokinesis.

Most bacterial species display a particular cellular morphology that is generally preserved across generations. The production and maintenance of shape require coordination among multiple cellular systems positioned at different places within the cell. The peptidoglycan cell wall, located external to the cytoplasmic membrane, is an important structural element that is required for shape maintenance. The processes governing the localization and timing of cell wall growth and turnover are likewise critical (8, 9, 23). The bacterial cytoskeleton is thought to play a central role in cell morphogenesis by exerting spatiotemporal control over peptidoglycan growth (8, 9, 23). In order for it to do so, there are numerous proteins that are required to connect cytoskeletal control mechanisms to the periplasmic enzymes that directly synthesize and modify the peptidoglycan cell wall. These proteins, such as MreC, MreD, RodA, and RodZ, are essential for maintenance of cell shape and are positioned in the cytoplasmic membrane to presumably link cytoskeletal elements in the cytoplasm to the activities of peptidoglycan-modifying enzymes in the periplasm (2, 5, 9, 23, 29). Some bacterial species also contain additional components that make important contributions to cell shape, such as cell wall teichoic acids in Gram-positive bacteria (9) and periplasmic flagella in spirochetes (41).

In the vibrioid bacterium *Caulobacter crescentus*, an intermediate filament-like protein, crescentin, is required for cell curvature (3). Crescentin forms an intracellular filamentous structure that is associated with the cell wall and is thought to mechanically govern cell wall growth to produce cell curvature (7). The crescentin structure is localized along the inner curvature of the cell under the cytoplasmic membrane (3, 7) and is highly stable, with no detectable subunit exchange (10). The association between the crescentin structure and the cell envelope appears essential for its function, since an attachment-defective crescentin mutant is unable to support cell curvature (7). The function of the actin-like protein MreB is also critical for the envelope association of the crescentin structure (10), and MreB may provide one part of the connection between the crescentin structure and the peptidoglycan cell wall.

Since bacterial morphogenesis requires multiple cellular components and systems, we used a genetic screen to find

* Corresponding author. Mailing address: Dept. of Molecular, Cellular and Developmental Biology, KBT 1032, Yale University, P.O. Box 208103, New Haven, CT 06520-8103. Phone: (203) 432-5170. Fax: (203) 432-9960. E-mail: christine.jacobs-wagner@yale.edu.

‡ These authors contributed equally to this work.

† Present address: Molecular Biology and Biochemistry Department, Wesleyan University, Middletown, CT 06459.

§ Supplemental material for this article may be found at http://jb.asm.org/.

▽ Published ahead of print on 30 April 2010.

other factors important for cell curvature in *C. crescentus*. Surprisingly, we found that an alteration in the lipopolysaccharide (LPS) biosynthesis pathway can have a catastrophic effect on the ability of the crescentin structure to associate with the cell envelope and govern cell curvature.

MATERIALS AND METHODS

Strains, plasmids, media, mutagenesis, and growth conditions. *C. crescentus* was grown at 30°C in PYE (peptone-yeast extract) or M2G supplemented with 1% PYE ($M2G^+$) (16). Vanillic acid (0.5 mM) or xylose (0.3%) was added to the medium to induce the P_{van} or P_{xyl} promoter, respectively, when appropriate. Plasmids were mobilized from *Escherichia coli* strain S17-1 into *C. crescentus* by conjugation (16) or electroporation. Plasmids and strains are listed in Table 1, and their construction and primers are described in the text of the supplemental material. Exponentially growing cultures were used for all experiments unless otherwise noted. For transposon mutagenesis, a plasmid bearing the mini-Tn*5* Km2 (LS1680) was mated into CJW940 or a plasmid bearing the Himar*1* element (pSC189) (11) was electroporated into CJW1034. UV mutagenesis was performed on strain CJW1126. Two 100-μl drops of an overnight culture (in stationary phase) were placed on a petri dish, set atop a Spectroline TVC-312R UV transilluminator, and irradiated for 40 s at the maximum intensity setting.

Light microscopy and photobleaching. Cells were imaged at room temperature (~22°C) or at 31°C using an objective heater on either a Nikon E1000 microscope fitted with 100× differential interference contrast (DIC) and phase-contrast objectives and a Hamamatsu Orca-ER LCD camera or a Nikon E80i microscope with similar objectives, an Andor iXon+ camera, and a Hamamatsu Orca-IIER LCD camera. The latter setup and the Andor camera were used for photobleaching with a Photonic Instruments Micropoint laser system with a 481-nm dye cell. Photobleaching was performed with 10 pulses with power 2 at the attenuator plate and 18% transmission at the internal attenuator, using an ND8 filter. Cells were immobilized on 1% agarose-PYE or $M2G^+$ agarose-padded slides containing vanillic acid or xylose inducers when appropriate. Immunofluorescence microscopy was performed as previously described (3) using anticrescentin antibodies at 1:800. Images were taken and analyzed with the Metamorph software program (MDS Analytical Technologies). For live-cell immunofluorescence, cells were incubated with 1:200 anti-"smooth" LPS (S-LPS) in PYE medium for 15 min at 30°C, washed twice with PYE, incubated with 1:200 fluorescein isothiocyanate (FITC)-conjugated goat anti-rabbit immunoglobulin in PYE for 15 min, washed twice with PYE, resuspended in $M2G^+$, and mounted on $M2G^+$-1% agarose pads for microscopy.

Cell curvature analysis. Automated cell curvature analysis was performed using Matlab as described previously (7). Briefly, cell outlines were obtained from phase-contrast images, and the center line of each cell was detected. In order to find the curvature of the cells, multiple points located equidistantly along the center line were fitted to an arc of a circle, minimizing the sum of the squared distances to the centerline points from their projections to the arc. The reciprocal of the radius of the best-fit arc is the curvature value. The few cells where the centerline shape was not representative of cell curvature (e.g., dividing cells that bend at the constriction site) were removed prior to statistical analysis by applying a cutoff to the curvature distribution. Statistical calculations were done using Matlab.

Gel staining and immunoblotting. Affinity-purified anticrescentin antibodies were used for immunoblotting at a dilution of 1:15,000. The load volume was normalized to optical density at 600 nm (OD_{660}) values. Polysaccharide isolation for LPS immunoblot analysis was performed as previously described (38). Specifically, cells were washed with 10 mM HEPES, pH 7.2, resuspended in 10 mM Tris–1 mM EDTA, and frozen in a volume of 250 μl. Samples were thawed, combined with 1 μl DNase (0.5 mg/ml), 20 μl lysozyme (10 mg/ml), and 3 μl 1 M $MgCl_2$, and incubated at room temperature for 15 min. The above mixture (38.75 μl) was then combined with 10 μl of 5× SDS dye, incubated at 100°C for 10 min, and cooled to room temperature. Proteinase K (1.25 μl of a 20-mg/ml stock solution) was added, and the sample was incubated at 60°C for 1 h. Samples were analyzed on 10% or 12% acrylamide gels by SDS-PAGE. Gels were silver stained according to a previously described method (36) with minor modifications (38). Blots were generally probed with anti-S-LPS antibodies (37) at a dilution of 1:100,000 for 15 to 30 min. For anti-RsaA (S-layer) blotting, total cell extracts (normalized by OD_{660}) or isolated shed material was used. Shed material was collected on a nylon mesh, washed extensively with 1 M Tris (pH 7.5), and then dissolved in 0.1 M Tris (pH 7.5)–8 M urea. Anti-RsaA was used at 1:10,000.

Sucrose gradient centrifugation. CB15N cells (800 ml) at an OD_{660} of 0.3 were pelleted (12,000 × *g*) and resuspended in 28 ml of 10 mM Tris (pH 7.5)–0.75 M sucrose at 4°C, at which temperature all the following steps were performed. Lysozyme was added to 50 μg/ml, an EDTA-free complete protease inhibitor cocktail tablet (Roche) was added, and then 56 ml of cold 1.5 mM EDTA (pH 7.5) was added dropwise with constant swirling. The cells were incubated on ice for 10 min before being lysed in a French press set to ~750 lb/in^2 (a very low pressure that results in only a fraction of the cells being lysed; higher pressures cause the formation of predominately mixed inner/outer membrane vesicles that cannot be separated by density). The lysate was cleared by centrifugation (16,000 × *g*), and the cleared lysate was ultracentrifuged at 160,000 × *g* for 1.5 h. The membrane pellet was resuspended by Dounce homogenization in 3.3 mM Tris (pH 7.5)–1 mM EDTA–0.25 M sucrose, and 500 μl was carefully laid over a 35 to 60% sucrose (in 5 mM EDTA [pH 7.5]) step gradient in Beckman-Coulter SW41 tubes. The tubes were centrifuged for 40 h at 140,000 × *g* at 4°C. Fractions (500 μl) were collected by hand, and 4 volumes of each fraction were mixed with 1 volume of 5× SDS loading buffer. The samples were separated by 10% PAGE, transferred to polyvinylidene difluoride (PVDF) membranes, and immunoblotted.

Muropeptide analysis. Sacculi were isolated from 1-liter PYE cultures grown without antibiotics at 30°C and harvested in mid-log phase (OD_{660} between 0.3 and 0.4). Under these conditions, CB15N doubles in 90 min, and CJW1090 and CJW1249 double in 95 min. Isolation, identification, and high-performance liquid chromatography (HPLC) analysis of muropeptides were performed as described previously (19) with previously published modifications (34).

RESULTS AND DISCUSSION

Identification of a gene required for cell curvature. To find genes involved in the generation or maintenance of normal cell morphology, we made libraries of mutant *C. crescentus* cells by UV or transposon mutagenesis. To increase the randomness of transpositions, we independently used either the Tn*5*-derived mini-Tn*5* Km2 or the *mariner*-based Himar*1*. We then visually screened these mutant libraries for cell shape defects by DIC microscopy. UV-generated mutations of interest were mapped by complementation using a cosmid library in a 96-well plate format, while transposon insertions were identified by cloning the transposon and surrounding sequence into a vector and by sequencing from the transposon sequence.

From more than 5,000 transposon mutants screened, 8 had a cell curvature defect. This defect was quantified by computerized image analysis (7) to obtain numerical values for cell curvature (see Materials and Methods). For comparison, wild-type cells have a median cell curvature of 0.39 μm^{-1} (Fig. 1A, panel ii), whereas crescentin-null mutant cells, which have virtually no detectable curvature, have a median cell curvature of 0.06 μm^{-1} (Fig. 1A, panel i). Four of the 8 mutants with curvature defects had a Tn*5* insertion in the crescentin-encoding gene *creS*. Transposon insertions in *rcdA*, encoding a CtrA degradation regulator, the gene *cc_0884*, encoding a predicted transcriptional regulator, and the cell division gene *ftsH* also produced cells with reduced curvature, but these mutants were elongated compared to the wild type (data not shown) and therefore were not analyzed further. However, a Himar*1* insertion in the gene *cc_0632* of hypothetical function produced cells with normal lengths but with a considerable reduction of cell curvature (0.2 μm^{-1}; Fig. 1A, panel iii).

The *cc_0632* gene is the penultimate gene of a predicted operon encompassing *cc_0635* to *cc_0631* (Fig. 1B), suggesting a potential polar effect on the downstream *cc_0631* gene. Consistent with this notion, a UV-generated mutant with a straight cell shape (0.11 μm^{-1}) was found to have a point mutation in *cc_0631* (Fig. 1A, panel v). A cosmid (cos1-10-A) containing

TABLE 1. Strains and plasmids

Strain or plasmid	Relevant genotype or description	Reference or source
C. crescentus		
CB15N	Synchronizable variant of CB15, also known as NA1000	17
CJW914	CB15N/pJS14P_{xyl}creS$_{\Delta N27}$	This study
CJW926	CB15N *pleC*::*pleC-yfp wbqL*(*W138R*)	This study
CJW940	CB15N *recA pleC*::*pleC-tdimer2*/pMR20divJ-myfp-divK-mcfp	This study
CJW1034	CB15N *recA cckA*::Ω *divJ*::pBGENTcckA-yfpdivJ-tdimer2/pMR20divL-cfp	This study
CJW1084	CB15N *pleC*::*pleC-yfp cc_0631*(*W138R*)/cos1-10-A	This study
CJW1090	CB15N *wbqL*::pBGENT-KO	This study
CJW1117	CB15N *wbqL*::pBGENT-KO/pMR20wbqL	This study
CJW1126	CB15N *pleC*::*pleC-yfp*/pMR10divK-cfp	This study
CJW1243	CB15N *wbqV*::Tn*5* (also known as mutant F3)	4
CJW1249	CB15N *wbqP*::Tn*5* (also known as mutant F24)	4
CJW1537	CB15N Δ*creS*/pMR20P_{xyl}creS$_{\Delta N27}$-tc	7
CJW1901	CB15N *wbqL*::Tn*5* (also known as mutant F26)	4
CJW1908	CB15N *wbqP*::Tn*5 wbqL*::pBGENT-KO	This study
CJW1917	CB15N *wbqP*::Tn*5 wbqL*::pBGENT-KO/pMR20tipN-wbqP	This study
CJW1930	CB15N *wbqV*::Tn*5 wbqL*::pBGENT-KO	This study
CJW1933	CB15N *cc_0632*::Himar*1*	This study
CJW1935	CB15N *cc_0632*::Himar*1*/pMR20wbqL	This study
CJW2861	CB15N *creS*::pHL23creS-mgfp	This study
CJW2876	CB15N *wbqL*::pBGENT-KO *creS*::pHL23creS-mgfp	This study
CJW3130	CB15N *ftsZ*:pXMCS7ftsZ *creS*::pHL23creS-mgfp *wbqL*::pBGENT-KO	This study
CJW3292	CB15N *ftsZ*::pBJM1 *wbqL*::pBGENT-KO	This study
CJW3295	CB15N *wbqL*::pBGENT-KO/pJS14creS-tc	This study
CJW3329	CB15N Δ*creS wbqL*::pBGENT-KO P_{van}::pBGENTP$_{van}$creS-tc::pHL32P$_{van}$creS-gfp	This study
CJW3330	CB15N/pJS14creS-tc	This study
CJW3332	CB15N *ftsZ*:pXMCS7ftsZ Δ*creS* P_{van}::pBGENTP$_{van}$creS-tc::pHL32P$_{van}$creS-gfp *wbqL*::pBGENT-KO	This study
JS1003	CB15N *rsaA*::KSac	15
LS3812	CB15N Δ*creS*	18
E. coli		
DH5α	Cloning strain	Invitrogen
CJW1014	DH5α λ*pir*+/pSC189	11
CJW1080	S17-1/cos1-10-A	Craig Stephens
CJW1082	S17-1/pMR20wbqL	This study
CJW1259	S17-1/pMR20P_{xyl}creS(ΔN27)-tc	This study
CJW1268	S17-1/pRK415	20
CJW1446	S17-1/pJS14creS-tc	This study
CJW1907	S17-1/pBGENT-KO	This study
CJW3363	S17-1/pMR20tipN-wbqP	This study
LS385	S17-1/pBGS18T	Lucy Shapiro
LS1680	S17-1 λ*pir*/pUT-mini-Tn*5* Km2	14
S17-1	M294::RP4-2 (Tc::Mu)(Km::Tn*7*); for plasmid mobilization	30
Plasmids		
cos1-10-A	Cosmid containing a ~20-kb chromosomal segment between coordinates 684666 and 715000 in the *C. crescentus* genome; contains genes *cc_0620-cc_0646*	Craig Stephens
pBGENT	Integration plasmid (Gen^r)	22
pBGENT-KO	pBGENT containing a 450-bp SacI/KpnI internal fragment of *wbqL* cloned into pBGENT for *wbqL* gene disruption by vector insertion	This study
pBGENTPvancreS-tc	pBGENT carrying *creS-tc* under the control of P_{van}	10
pBJM1	pBGST18T carrying a 5′ portion of *ftsZ* ORF under the control of P_{xyl}[a]	39
pHL23	Integration plasmid (Kan^r)	21
pHL23creS-mgfp	pHL23 carrying an insert coding for crescentin with a C-terminal fusion of monomeric GFP	This study
pHL32PvancreS-gfp	pHL32 carrying *creS-gfp* under the control of P_{van}	10
pJS14	Chl^r pBBR1-derived medium-copy-no. broad-host-range vector	Jeffrey Skerker
pJS14creS-tc	pJS14 carrying the *creS-tc* gene	This study
pJS14PxylcreSΔN27	pJS14 carrying *creS*(Δ*N27*) under the control of the xylose-inducible promoter	This study
pKS (Bluescript)	Amp^r cloning vector	Stratagene
pMR10	Tet^r low-copy-no. broad-host-range vector	Richard Roberts
pMR10divK-cfp	pMR10 carrying *divK-cfp*	This study
pMR20	Tet^r low-copy-no. broad-host-range vector	28
pMR20divJ-myfp-divK-mcfp	pMR20 carrying *divJ-myfp* and *divK-mcfp*	22
pMR20divL-cfp	pMR20 carrying *divL-cfp*	This study
pMR20P_{xyl}creS(ΔN27)-tc	pMR20 carrying *creS*(Δ*N27*)*-tc* under the control of the xylose-inducible promoter	7
pMR20wbqL	pMR20 carrying the *wbqL* gene	This study
pMR20tipN-wbqP	pMR20 carrying the *tipN* and *wbqP* genes	This study
pRK415	Unstable Tet^r plasmid in *C. crescentus*	20
pRK415wbqL	pRK415 carrying the *wbqL* gene	This study
pSC189	Delivery plasmid bearing the Himar*1* transposon	11
pXMCS7ftsZ	pXMCS7 carrying *ftsZ* under the control of P_{xyl}	10
pUT-mini-Tn*5* Km2	pUT delivery plasmid carrying the mini-Tn*5* transposon	14

[a] ORF, open reading frame.

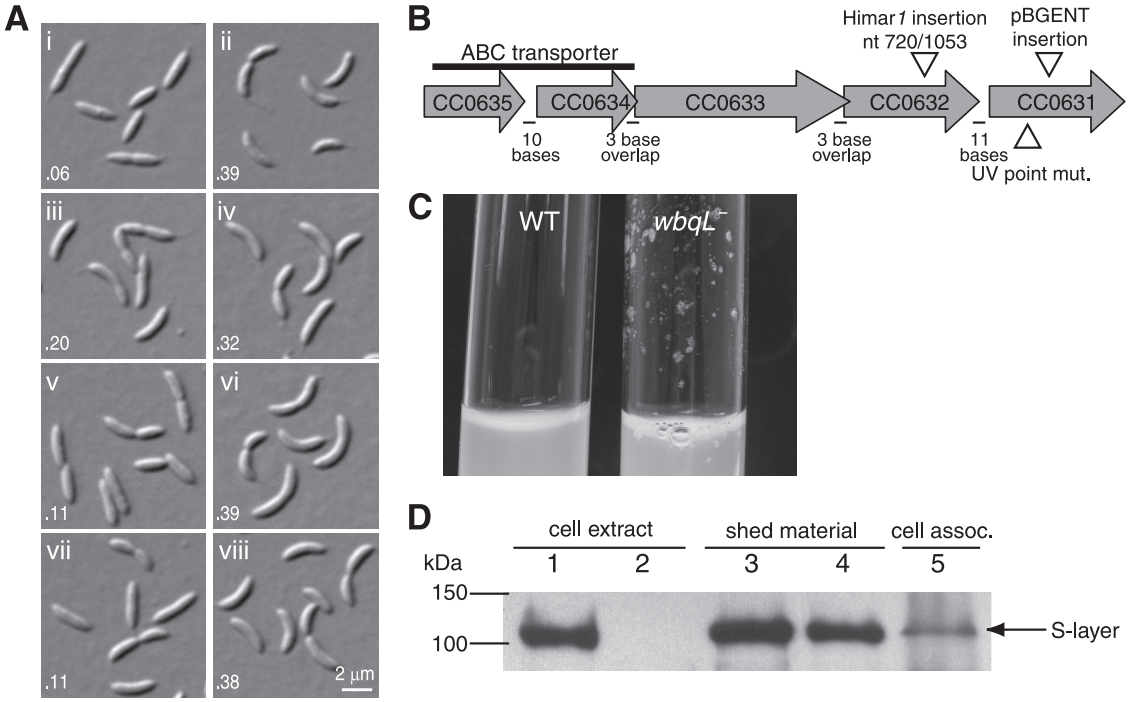

FIG. 1. Mutations in *cc_0631* cause cell curvature and S-layer shedding defects. (A) Differential interference contrast (DIC) images of transposon or point mutants found in a screen for cell curvature loss and the same mutants when complemented with extra copies of the wild-type genes on plasmids or cosmids. i, straight rod-shaped Δ*creS* cells; ii, wild-type cells; iii, *cc_0632*::Himar*1* mutant cells (CJW1933); iv, *cc_0632*::Himar*1* cells expressing *cc_0631* from a low-copy-number plasmid (CJW1935); v, *cc_0631*(W138R) cells (UV mutant; CJW926); vi, *cc_0631*(W138R) cells carrying a cosmid, cos1-10-A, containing *cc_0631* and flanking regions (CJW1084); vii; cells in which *cc_0631* has been disrupted by insertion of plasmid pBGENT-KO (CJW1090); viii, *cc_0631*::pBGENT-KO cells expressing *cc_0631* from low-copy-number plasmid pMR20 (CJW1117). Quantified cell curvature values for each strain are in the lower left corner of each image. (B) Schematic representation of chromosomal gene arrangement with the locations of mutations or transposon insertions indicated. (C) Photograph of stationary-phase wild-type and *cc_0631*::pBGENT-KO (CJW1090) liquid cultures after growth overnight in PYE medium. (D) Anti-S-layer immunoblot of material shed into the culture medium by the *cc_0631* point and insertion mutants. Blots of whole-cell extracts from the wild type (WT) (CB15N; lane 1) and an *rsaA* mutant that does not produce S layer (lane 2) are shown for reference. Lanes 3 and 4 show isolated shed material from *wbqL* mutants (CJW926 and CJW1090, respectively). Lane 5 shows a whole-cell extract from washed *wbqL* mutant cells (CJW1090) after removal of shed material.

cc_0631 and flanking regions complemented the UV mutant (0.39 μm^{-1}; Fig. 1A, panel vi), whose point mutation in *cc_0631* should have no effect on the expression of *cc_0632*. Additionally, the *cc_0632*::Himar*1* cell shape defect could be rescued with a plasmid bearing the *cc_0631* sequence driven by P_{lac} (0.32 μm^{-1}; Fig. 1A, panel iv), suggesting that a polar effect on the expression of *cc_0631* was responsible for the moderate curvature defect of *cc_0632*::Himar*1* cells. To confirm this, we specifically interrupted the *cc_0631* gene by plasmid insertion (generating strain CJW1090) (Fig. 1A, panel vii). This gene disruption resulted in the same loss of curvature as observed for the UV mutant (0.11 μm^{-1}) and could be complemented by plasmid-borne *cc_0631* (0.38 μm^{-1}) (Fig. 1A, panel viii). Collectively, these results indicate that the proper functioning of the *cc_0631* gene product is required for cell curvature.

Loss of cell curvature is accompanied by altered O-polysaccharide and S-layer shedding. We noticed that stationary-phase liquid cultures of *cc_0631* mutant cells contained debris that was visible on the sides of culture tubes (Fig. 1C). In *C. crescentus*, the surface of the cell is covered by an S layer, a hexagonal protein lattice (32). Since there are some *C. crescentus* mutants that are known to shed S-layer proteins (37), we tested to see whether this debris contained S layer, which is made of the RsaA protein (15, 31). Immunoblots of whole-cell extracts of wild-type CB15N cells displayed a clear band of RsaA at ~130 kDa (15) (Fig. 1D, lane 1), while cells with an antibiotic resistance cassette in the *rsaA* gene (JS1003) lacked detectable protein (Fig. 1D, lane 2). Along with these controls, we analyzed the debris shed by the *cc_0631* disruption mutant and the *cc_0631* UV mutant. The debris was isolated from stationary-phase cultures on nylon mesh, washed, and solubilized in urea. The lanes containing this debris exhibited the characteristic RsaA band (Fig. 1D, lanes 3 and 4), showing that the shed material contained S layer. Some S-layer material remained associated with the cell (Fig. 1D, lane 5).

Since the paracrystalline array of S-layer protein is attached to the cell surface through the O-polysaccharide portion of lipopolysaccharide (LPS) in the outer membrane and since mutants in LPS synthesis shed S layer (37), we tested whether *cc_0631* mutants produced altered LPS. To do so, we used an antibody that is specific for "smooth" LPS (S-LPS) (37). S-LPS is composed of lipid A, to which core sugar and O-polysaccharide are linked. Since this antibody does not recognize "rough" LPS containing only lipid A and core sugar (26), we assume that this antibody is specific for the O-polysaccharide portion of LPS. In *Escherichia coli*, the lipid-bound core and O-antigen oligosaccharides are synthesized separately at the inner face of

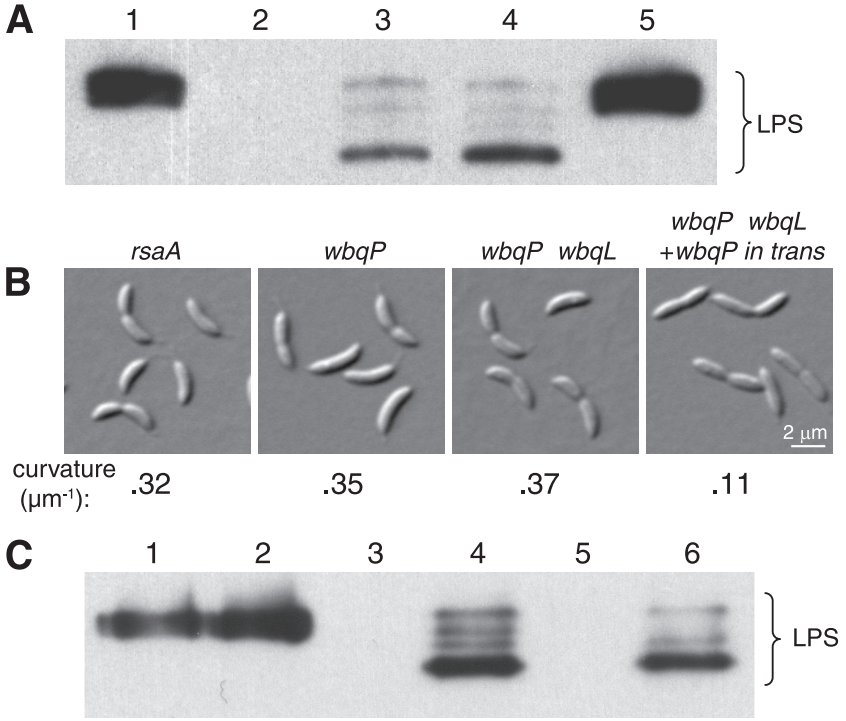

FIG. 2. Altered O-antigen species, and not the synthesis of O antigen or S layer, causes the loss in cell curvature. (A) Anti-O-antigen immunoblot of extracts prepared from wild-type (CB15N; lane 1), O-antigen-null (*wbqP*::Tn*5*; CJW1249; lane 2), *wbqL*(W138R) mutant (CJW926; lane 3) or *wbqL*::pBGENT mutant (CJW1090; lane 4) cells or *wbqL*::pBGENT-KO cells complemented with *wbqL* expressed from pMR20 (CJW1117; lane 5). Loading for all immunoblots in this figure was normalized by OD_{660} values. (B) DIC images of cells lacking S layer (*rsaA*::KSac; JS1003), lacking O-antigen production (*wbqP*::Tn*5*; CJW1249), lacking O-antigen production but also carrying *wbqL*::pBGENT-KO (CJW1908; *wbqP wbqL* mutant), or *wbqP*::Tn*5 wbqL*::pBGENT-KO with *wbqP* expressed from pMR20 (CJW1917). Quantified curvature values are given below each image. (C) Anti-O-antigen immunoblot of the strains shown in the images in panel B and reference strains: lane 1, wild type; lane 2, *rsaA*::KSac strain; lane 3, *wbqP*::Tn*5* strain; lane 4, *wbqL*::pBGENT-KO strain; lane 5, *wbqP*::Tn*5 wbqL*::pBGENT-KO strain; lane 6, *wbqP*::Tn*5 wbqL*::pBGENT-KO strain with *wbqP* expressed from pMR20.

the cytoplasmic membrane before being flipped onto the periplasmic face (40). There, multiple O-antigen oligosaccharides are ligated to the lipid-bound core, which is then shuttled to the outer membrane (24). Anti-O-polysaccharide immunoblots of *C. crescentus* polysaccharide extracts typically display a single band, corresponding to a homogeneous O-polysaccharide length (37). We confirmed this length homogeneity in wild-type cells (Fig. 2A, lane 1). As a negative control, we used a transposon mutant of *wbqP* (4) that does not produce a detectable O-polysaccharide band (lane 2, Fig. 2A). Consistent with an absence of O-polysaccharide, WbqP has been proposed, based on sequence homology, to initiate the formation of O-polysaccharide in the cytoplasm by conjugating the first sugar to the undecaprenol lipid carrier (4). Both *cc_0631* mutants (UV-generated and gene disruption; lanes 3 and 4 in Fig. 2A, respectively) showed heterogeneity in O-polysaccharide length, with multiple bands of shorter length than that for the wild type, with the shortest band being the most abundant. Addition of *cc_0631* on a low-copy-number plasmid in the *cc_0631* disruption mutant (strain CJW1117) restored both wild-type cell curvature (Fig. 1A, panel viii) and wild-type O-polysaccharide length uniformity (Fig. 2A, lane 5). These data indicate that the CC0631 protein plays a role in LPS biosynthesis in *C. crescentus* and that defects in LPS production are responsible for the S-layer shedding phenotype of *cc_0631* mutants.

Prior to this work, a screen had been performed to identify mutants that were defective in attachment of the S layer (4). Through this screen, a *wbqL* transposon mutant was identified (4). At the time, the mutant was characterized, but the sequence or reference number of the *wbqL* gene was not made publicly available until after we had determined, by comparing the gene length and those of neighboring genes, that their mutation was in *cc_0631*, which will here be called *wbqL*. Awram and Smit (4) showed that a *wbqL*::Tn*5* mutant sheds S layer and produces altered LPS but made no mention of a defect in cell shape. We confirmed that their *wbqL*::Tn*5* mutant had the same curvature defect that we observed with our *wbqL* mutants (data not shown).

BLAST alignment of the predicted WbqL protein sequence revealed that it matches the COG4421 superfamily of bacterial capsular polysaccharide biosynthesis proteins and shows substantial homology to a number of these proteins. The UV point mutation in *wbqL* that abolishes cell curvature (Fig. 1A, panel v) causes a tryptophan-to-arginine substitution at position 138 (W138R). Tryptophan 138 is located in a region of the sequence displaying high levels of conservation among different polysaccharide biosynthesis proteins (data not shown), in ac-

cord with this substitution affecting protein function. Consistent with an earlier alignment analysis suggesting that WbqL is a glycosyltransferase (4), HHpred structural prediction analysis (33) matched WbqL to general glycosyltransferase structure as well as to *E. coli* WaaF, which is ADP-heptose-LPS heptosyltransferase II. WaaF is responsible for ligating the second heptose unit to the core sugar of *E. coli* LPS (25). The composition of the core sugar of *C. crescentus* LPS is slightly different from *E. coli* (27), and its assembly pathway has not yet been determined. Because genes putatively involved in *C. crescentus* LPS biosynthesis have been identified solely based on abnormal or absent LPS in mutants and by sequence comparison to known LPS biosynthesis proteins (4), it is difficult to assign WbqL a specific function in LPS biosynthesis. In any case, it is clear that without WbqL, the cells accumulate an aberrant O-polysaccharide species (4).

Altered O-polysaccharide but not absence of O-polysaccharide or S layer results in cell curvature loss. Since the altered LPS species and associated S-layer shedding in *wbqL* mutant strains were correlated with a straight cell shape, we next examined whether cell curvature required the production of either S layer or O-polysaccharide. To test the dependence of curvature on S layer, we used an *rsaA* mutant strain (JS1003). These cells, which produce no detectable S layer (Fig. 1D, lane 2), had a curvature value of 0.32 μm^{-1} (Fig. 2B), which is close to the wild-type value (0.39 μm^{-1}). Therefore, cell curvature does not require S-layer production. Similarly, synthesis of O-polysaccharide is dispensable for cell curvature, since *wbqP*::Tn*5* cells (CJW1249) displayed near-normal curvature (0.35 μm^{-1}) (Fig. 2B).

Even though *wbqL* mutants shed the S layer and have altered O-polysaccharide, disruption of S layer or O-polysaccharide synthesis does not result in a defect in cell curvature. It was not clear whether the alteration in O-polysaccharide was directly related to the cell curvature defect. It was possible that WbqL might have a second role, unrelated to O-polysaccharide synthesis, which might result in the straight-rod shape in the *wbqL* mutant. Because *wbqP* mutant cells do not produce any detectable O-polysaccharide, *wbqP* would be predicted to be upstream of *wbqL* in the pathway of O-polysaccharide biosynthesis. We therefore created a *wbqP wbqL* double mutant (CJW1908), which would produce no O-polysaccharide (and therefore no altered O-polysaccharide either), and examined the shape of the cells. If a *wbqP* mutation in the *wbqL* null background could restore wild-type curved cell morphology, this would indicate that the altered O-polysaccharide species likely causes the straight-rod shape. If a *wbqP* mutation in the *wbqL* null background could not rescue wild-type curved cell morphology, this would support a model in which WbqL has dual roles, and the abrogation of WbqL's second role would cause the straight-rod shape independently from its effect on LPS.

The *wbqP wbqL* double mutant strain exhibited curvature (0.37 μm^{-1}) virtually indistinguishable from that of the wild type (Fig. 2B) and did not produce any detectable O-polysaccharide (Fig. 2C, lane 5). Supplying *wbqP* on a low-copy-number plasmid in this strain background (CJW1917) allowed the production of the aberrant O-polysaccharide species (Fig. 2C, lane 6) and led to cell curvature loss (0.11 μm^{-1}; Fig. 2B) identical to that of a *wbqL* mutant alone (Fig. 1A, panel vii).

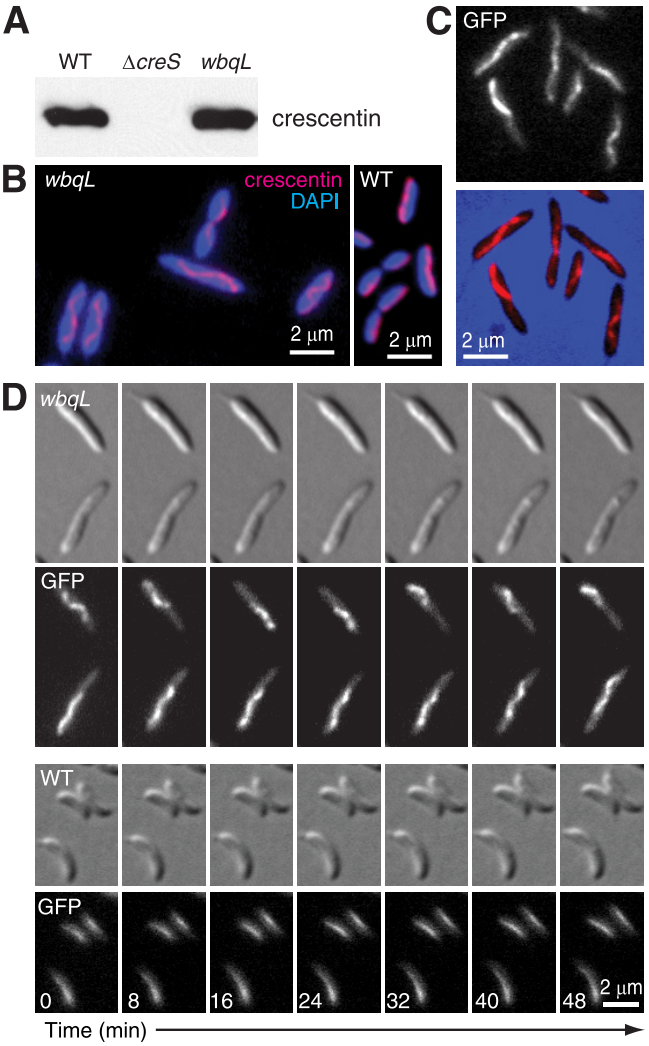

FIG. 3. Loss of cell curvature is caused by dissociation of the crescentin structure from the cell envelope. (A) Anticrescentin immunoblot of cell extracts from wild-type CB15N, crescentin-null Δ*creS*, or *wbqL*::pBGENT-KO strains. Loading was normalized by OD_{660} values. (B) Anticrescentin immunofluorescence (red) micrograph of mCB15N *wbqL*::pBGENT-KO (CJW1090; left panel) or wild-type CB15N cells (right panel). 4′,6-Diamidino-2-phenylindole (DAPI) counterstain is shown in blue. (C) Fluorescence micrograph of mGFP-labeled crescentin structures in CB15N *creS*::pHL23creS-mgfp *wbqL*::pBGENT-KO (CJW2876) cells. Overlay with phase-contrast image (blue) is also shown. (D) Top panel: DIC and GFP images from a time-lapse series showing the motion of mGFP-labeled crescentin structures in CJW2876 cells. Bottom panel: control time-lapse series from CB15N *creS*::pHL23creS-mgfp (CJW2861) cells.

This result suggested that it is the generation of an altered O-polysaccharide species, rather than the loss of normal O-polysaccharide, that causes the curvature defect. This strongly argues against a secondary function of WbqL that specifically relates to cell curvature, instead suggesting that a loss of cell curvature in a *wbqL* mutant is specifically due to the production of an altered O-polysaccharide species.

The crescentin structure does not associate with the cell envelope in a *wbqL* mutant. Since crescentin plays an essential role in cell curvature, we asked whether crescentin production, structure, or function was disrupted in *wbqL* mutants. Immu-

noblot analysis showed that crescentin was present in *wbqL* mutant extracts, with no visible degradation or size shift (Fig. 3A), indicating that the cell curvature defect was not caused by the absence or degradation of crescentin. Immunofluorescence microscopy revealed that while crescentin formed filamentous structures in *wbqL* mutant cells, these structures were S shaped and seemingly in the cytoplasm (Fig. 3B) instead of being linear and membrane juxtaposed along one side of the cells as seen in wild-type cells (3). This mislocalization was also visible in live cells (CJW2876) when crescentin was coproduced with monomeric green fluorescent protein-tagged crescentin (crescentin mGFP, which labels the endogenous crescentin structure [3]) (Fig. 3C). This localization pattern was reminiscent of envelope-dissociated crescentin structures generated by drug treatment or crescentin truncation (7, 10). We reasoned that such dissociated structures should display increased mobility within the cell, as previously observed (7, 10). Time-lapse imaging of mGFP-labeled crescentin structures revealed visible mobility within these cells (Fig. 3D). Thus, the loss of curvature in *wbqL* mutant cells is caused by a defect in the association of the crescentin structure with the cell envelope.

Collectively, our data suggest that an altered O-polysaccharide species in a *wbqL* mutant interferes with the association of the crescentin structure and the cell envelope. How might this interference occur? Since very little is known about LPS biogenesis in *C. crescentus*, we can only speculate. O-polysaccharide can still be exported in *wbqL* mutant cells, as evidenced by the presence of anti-O-polysaccharide-accessible epitopes on the surfaces of intact cells (see Fig. S1 in the supplemental material). However, it is unclear whether these epitopes represent the aberrant O-polysaccharide species or the small amount of normal-length O-polysaccharide produced in the mutant (Fig. 2C). As previously observed (4), silver staining for LPS revealed a faster-migrating band in the *wbqL* mutant that stained with intensity similar to that of the wild type (see Fig. S2 in the supplemental material). Since undecaprenyl-linked O-antigen precursors in *E. coli* have been reported to stain less efficiently than lipid A-linked LPS with silver (35), this raises the possibility that the aberrant band in the *wbqL* mutant represents a mature (lipid A-linked) LPS species that has been exported to the cell surface. Without more information, it is difficult to envision how an exported (i.e., noncytoplasmic) aberrant LPS product could interfere with the cytoplasmic crescentin structure.

Interference could be indirect, and we considered an effect on the peptidoglycan, since chemical perturbations of peptidoglycan synthesis can cause a similar phenotype of crescentin structure detachment (7, 10). However, the HPLC profiles of peptidoglycan digests (muropeptides) of wild-type, *wbqL* mutant, and *wbqP* mutant cells were very similar (Fig. 4A), showing identical peptidoglycan cross-linking and only a minor increase in glycan chain length in the *wbqL* mutant relative to the wild type (Fig. 4B; see also Tables S1 and S2 in the supplemental material). Since this small increase was also present in a *wbqP* mutant, which produces no LPS and has normal crescentin structure localization and function, these data strongly argue against a perturbation in peptidoglycan structure or synthesis interfering with crescentin structure localization in the *wbqL* mutant. Still, it remains possible that some aberrant LPS intermediates might be inefficiently exported across the cytoplasmic membrane, causing them to accumulate on the inner face of the cytoplasmic membrane, where they might interfere with the crescentin structure. Direct evidence for such a disruptive interaction is difficult to obtain, since membrane fractionation methods do not differentiate between membrane leaflets, and overlap of inner and outer membrane peaks is exacerbated in *wbqL* mutants (data not shown), complicating interpretation. However, in membrane fractionation of wild-type cells, a faster-migrating O-polysaccharide band detectable by anti-S-LPS is enriched in cytoplasmic-membrane fractions (see Fig. S3 in the supplemental material). This result raises the possibility that the faster-migrating band may represent an intermediate that normally faces the cytoplasm. If such intermediates accumulated in *wbqL* mutant cells, they might conceivably occlude or disrupt interactions between the crescentin structure and cytoplasmic membrane-associated factors that keep the crescentin structure localized at the cell envelope.

While the precise mechanism disrupting the crescentin structure localization in *wbqL* mutants remains speculative, we clearly show that a mutation altering LPS biosynthesis affects crescentin-mediated cell curvature. The intersection of these two usually unrelated cellular processes highlights the importance of physiological balance in cells. Perturbation of one pathway can upset this balance, possibly leading to production of an aberrant product and inducing a novel, disruptive interaction with another cellular component. Disruptive interactions of this kind have also been reported for other systems. In *Staphylococcus aureus*, disruptions in the teichoic acid biosynthesis pathway that are usually lethal are bypassed if the first enzyme in the pathway is inactivated (13). In this case, aberrant buildup of toxic teichoic intermediates is probably at play, possibly analogous to the aberrant O-polysaccharide species seen in a *wbqL* mutant. Similarly, an O-polysaccharide transporter knockout in *E. coli* inhibits cell growth and division but not when a gene upstream in the synthesis pathway is inactivated (12). The potential for creating harmful interactions may be an evolutionary constraining force, favoring changes that refine the harmony between different cellular systems as an organism adapts to its environment.

Envelope-dissociated crescentin blocks cell division when overproduced. The dissociation of crescentin structures in a *wbqL* disruption background provides a useful tool for probing the configuration and behavior of dissociated crescentin structures in the absence of crescentin mutations or drug treatments. Consistent with earlier reports (7, 10), we observed primarily left-handed (91%; $n = 204$) helical structures by both immunofluorescence and mGFP tagging in elongated cells made by depleting the cell division protein FtsZ (Fig. 5A to C). Addition of new crescentin subunits along the entire length of the crescentin structure was independent of envelope association (data not shown). Similarly, biphasic growth, where longitudinal extension is replaced by primarily lateral thickening once crescentin structures reach the cell poles (10), was normal and thus independent of membrane association in the *wbqL* mutant (data not shown).

During normal cell division in *C. crescentus*, the crescentin structure is cleaved or locally depolymerized at the division site so that each daughter cell inherits part of the crescentin structure. This process works well even when crescentin (tagged with a tetracysteine motif [TC]) is strongly overproduced from

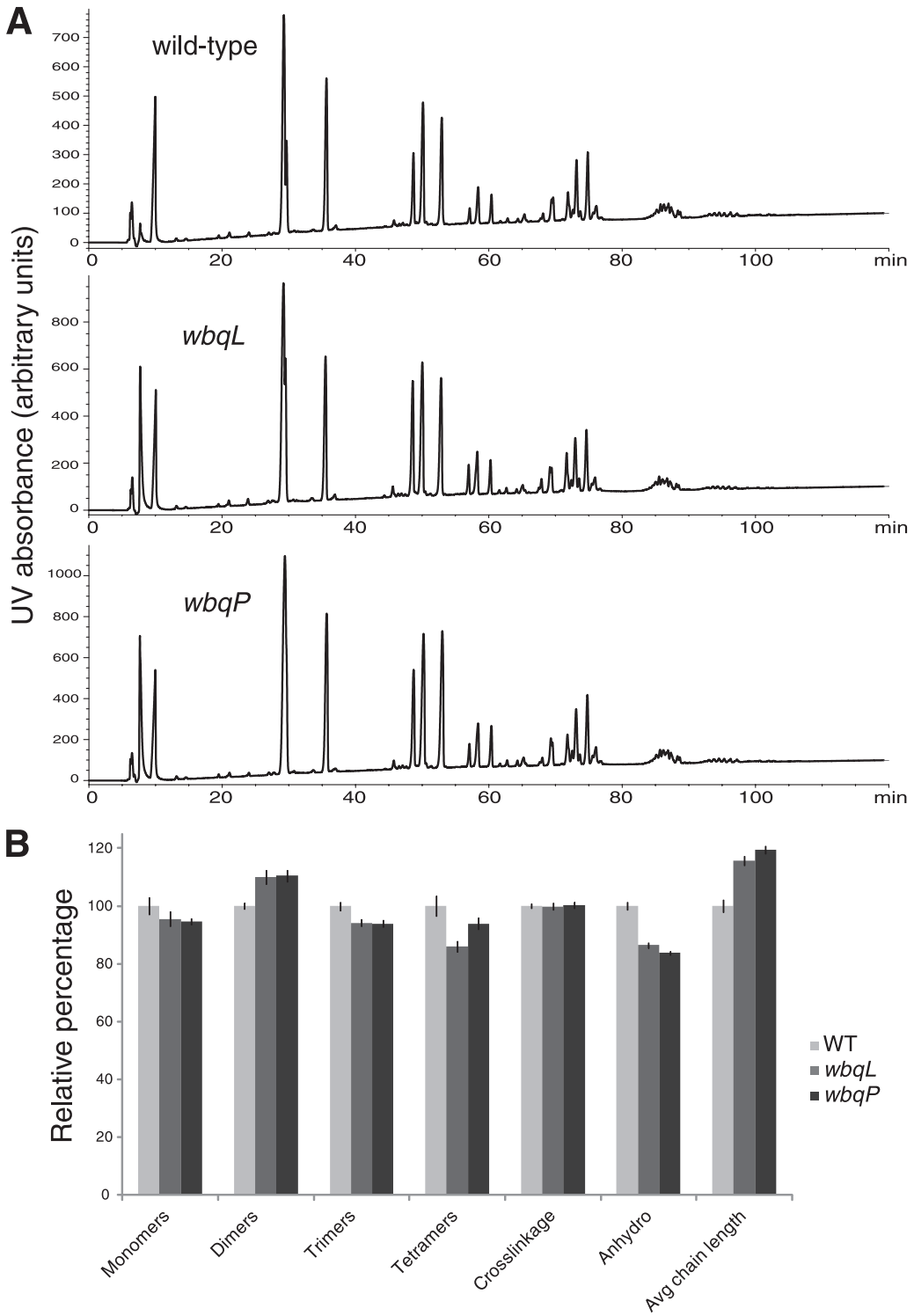

FIG. 4. Muropeptide analysis of wild-type and *wbqL* mutant peptidoglycan. Muropeptide analysis was performed for wild-type (CB15N), *wbqL*::pBGENT-KO (CJW1090), and *wbqP*::Tn*5* (CJW1249) strains. The *wbqP* mutant strain was used as a control, since this strain (CJW1249) does not produce any detectable LPS but shows normal crescentin structure localization and function. (A) Chromatographic traces of HPLC-separated muropeptides from the three strains. (B) Comparison of the abundance of each cross-linked muropeptide species, the overall cross-linking percentage, the abundance of anhydro glycan ends, and the average glycan chain length. The values are expressed as percentages of the wild-type value. The data reflect the means of results from two independent experiments; error bars represent standard deviations. The numerical values for the data shown in this panel are given in Table S1 in the supplemental material, and the abundance of each individually identified muropeptide species is listed in Table S2.

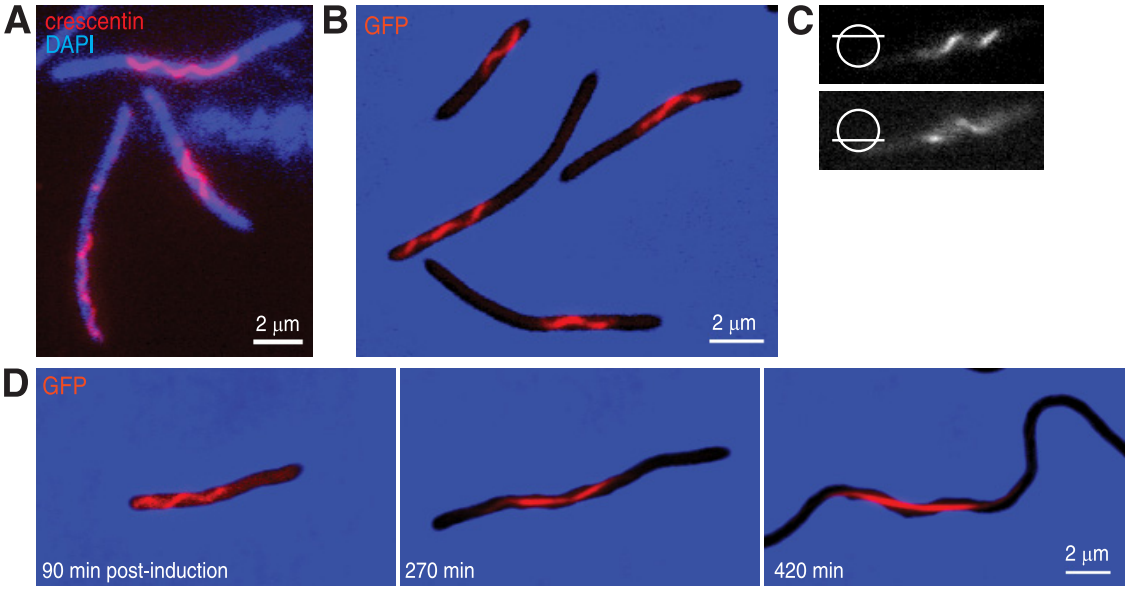

FIG. 5. Cell envelope-dissociated crescentin structures adopt a helical configuration. (A) Anticrescentin immunofluorescence (red) micrograph of CB15N *ftsZ*::pBJM1 *wbqL*::pBGENT-KO (CJW3292) cells depleted of FtsZ for 4.3 h. DAPI counterstain is shown in blue. (B) Fluorescence micrograph of GFP-labeled crescentin structures in CJW3130 (CB15N *ftsZ*:pXMCS7ftsZ *creS*::pHL23creS-mgfp *wbqL*::pBGENT-KO) cells elongated by depletion of FtsZ for 3.5 h. Crescentin-mGFP (red) is laid over a phase-contrast image (blue). (C) Optical sections of a CJW3130 cell to show helical handedness of the mGFP-labeled crescentin structure. (D) Time-lapse images of CJW3332 (CB15N *ftsZ*:pXMCS7ftsZ Δ*creS* P_{van}::pBGENTP$_{van}$creS-tc::pHL32P$_{van}$creS-gfp *wbqL*::pBGENT-KO) cells. The cells are producing crescentin-TC and crescentin-GFP *de novo* (due to the presence of vanillic acid inducer) under FtsZ depletion conditions (due to the absence of xylose), so that the cells do not divide during induction of crescentin-TC and crescentin-GFP synthesis.

a medium-copy-number plasmid, pJS14 (Fig. 6A). We therefore tested whether the cell division-dependent disruption of the crescentin structure was related to envelope association. We similarly produced crescentin-TC from pJS14 in a *wbqL* disruption background (CJW3295). In these *wbqL* mutant cells, the overproduced crescentin-TC formed a brightly fluorescent, nearly straight filamentous structure within cells (Fig. 6B). The straight rather than helical configuration of the crescentin-TC structure likely results from crescentin overproduction, since dissociated crescentin structures in FtsZ-depleted cells (CJW3332) also tend to lose their helicity during the course of overproduction (Fig. 5D). This loss of crescentin structure helicity may be due to its becoming stiffer as a result of continued lateral addition of crescentin subunits.

Overproduction of crescentin in *wbqL* mutant cells also caused a striking cell chaining phenotype, with many cells in the population appearing to be linked together by a single crescentin structure (Fig. 6B). Additionally, thin cellular extensions, visible by phase-contrast microscopy, appeared to link some chained cells together (Fig. 6B, arrowheads). These extensions often contained a crescentin-TC structure (Fig. 6B, inset), suggesting that the presence of a dissociated, thicker crescentin structure caused a block in cell division. However, it was also possible that this inability of cells to divide efficiently in the presence of a thick crescentin structure was specific to the inactivation of *wbqL*. To rule this out, we used an N-terminally truncated mutant of crescentin, crescentin$_{\Delta N27}$, which is able to form a filamentous structure but is dissociated from the cell envelope (7). We overexpressed *creS*(*ΔN27*)*-tc* using the P_{xyl} promoter on the low-copy-number plasmid pMR20 in a crescentin-null background (CJW1537), so that it was the only source of crescentin in the cell. Upon induction of crescentin$_{\Delta N27}$-TC production, a strong cell chaining phenotype developed. Just as in the *wbqL* mutant background, crescentin$_{\Delta N27}$-TC filamentous structures were straight (consistent with overproduction) and spanned the length of multiple chained cells (Fig. 6C). The cell chains displayed clear constrictions that contained crescentin$_{\Delta N27}$-TC structures (Fig. 6C, arrows), giving the impression that the cells had attempted to divide but could not separate the crescentin structure.

Since crescentin has not yet been conclusively identified in electron cryotomography (ECT) experiments (6), we reasoned that the thinness of these crescentin$_{\Delta N27}$-containing constrictions, combined with protein overproduction, might allow good visualization of the crescentin$_{\Delta N27}$ structure. Indeed, ECT revealed thick and straight filament bundles within the cytoplasm of cells that were sometimes bent at stalled division sites (Fig. 6D). In the image shown, the division site appears to have constricted until it reached the approximate diameter of the crescentin bundle but no further. Fully developed flagellar motors (FM, Fig. 6D) and chemoreceptor arrays (CR, Fig. 6D) are present at each side of the constriction, as might be expected if daughter cells failed to separate but then advanced through their respective cell cycles. Collectively, these data suggest that the thicker crescentin structures formed by crescentin overproduction interfere with the completion of cytokinesis when they are dissociated from the cell envelope.

How might envelope association assist in successful division of the crescentin structure during cell division? One possibility is that a protein or factor that promotes degradation or disassembly of crescentin filaments at the division site is membrane associated and therefore cannot act efficiently on the crescen-

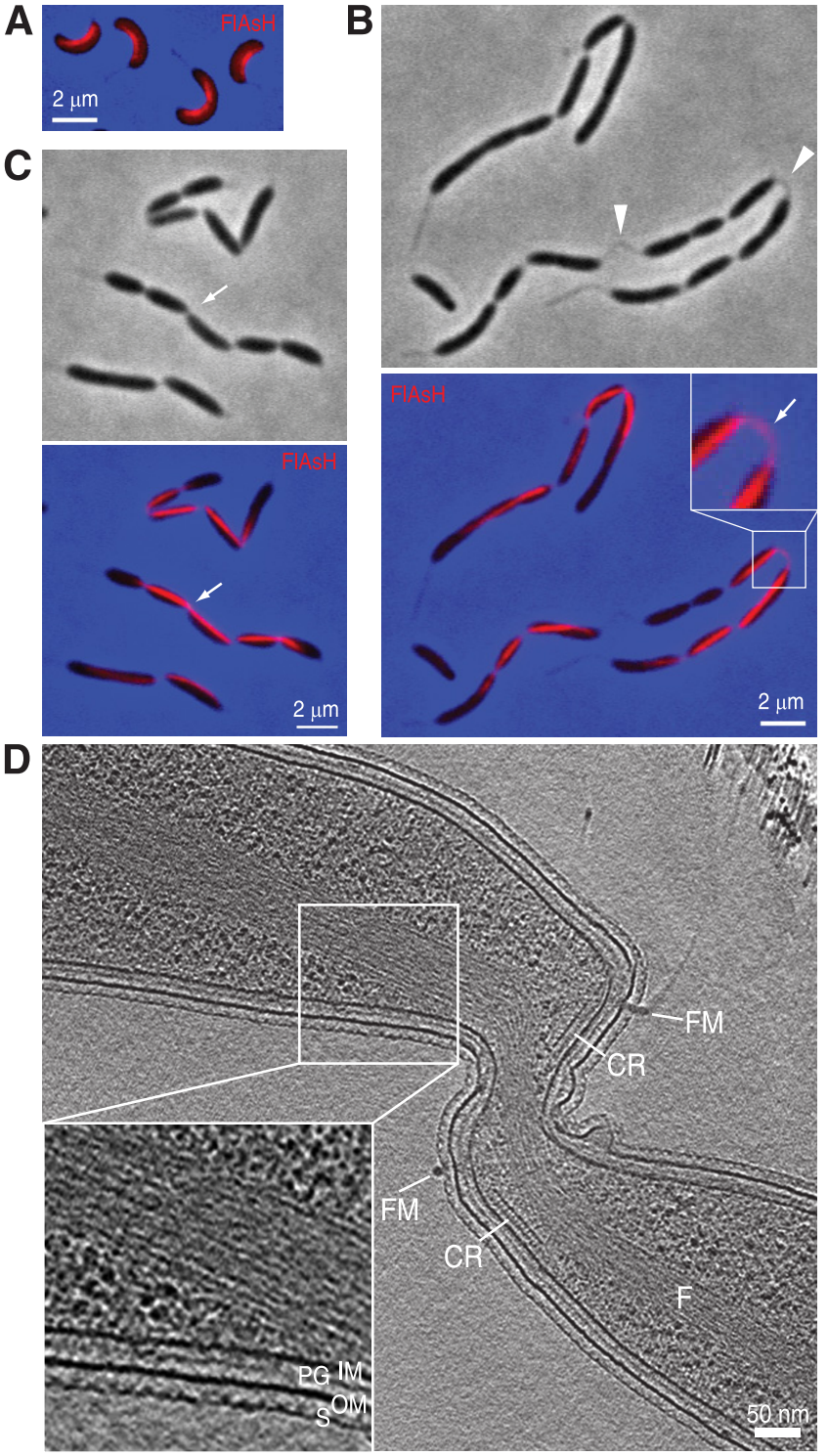

FIG. 6. Overproduction of envelope-dissociated crescentin causes cell chaining. (A) Image of fluorescein arsenical helix binder (FlAsH)-labeled crescentin-TC (red) overproduced in a wild-type background (CJW3330; CB15N/pJS14creS-tc cells), laid over phase-contrast micrograph (blue). (B) Micrographs of cells overproducing crescentin-TC in a *wbqL*::pBGENT-KO background (CJW3295; CB15N *wbqL*::pBGENT-KO/pJS14creS-tc). Phase-contrast image is given at top, with an overlay of phase-contrast (blue) with FlAsH-stained crescentin-TC (red) at bottom. Arrowheads indicate visible thin extensions connecting chained cells; inset magnifies the presence of a visible crescentin structure running through one such extension (arrow). (C) Images of FlAsH-stained crescentin$_{\Delta N27}$-TC (red) overproduced (induced for 4 h) as the only source of crescentin in the cell [CJW1537; CB15N Δ*creS*/pMR20P$_{xyl}$creS(ΔN27)-tc], laid over phase-contrast micrograph (blue). Arrow indicates a crescentin$_{\Delta N27}$-TC structure running between chained cells. (D) Section of an electron cryotomogram of two chained CJW914 cells [CB15N/pJS14P$_{xyl}$creS(ΔN27)] overproducing crescentin$_{\Delta N27}$. F, filamentous structure; CR, chemoreceptor array; FM, flagellar motor; S, S layer; OM, outer membrane; PG, peptidoglycan; IM, inner membrane.

tin structure when this structure is dissociated from the membrane, as in a *wbqL* mutant. Interestingly, *E. coli* displays a cell chaining defect when crescentin is exogenously expressed even though the crescentin structure is envelope associated (7). It is therefore possible that the evolutionarily distant *E. coli* lacks an important factor for splitting the crescentin structure during division. *C. crescentus* also exhibits a considerable period of midcell elongation preceding division that is not shared by *E. coli* (1). It is tempting to hypothesize that midcell elongation in *C. crescentus* would tend to stretch the envelope-associated crescentin structure, making its disruption at the division site more favorable.

ACKNOWLEDGMENTS

We thank J. Smit for gifts of strains, anti-O-polysaccharide, and anti-RsaA antibodies, O. Sliusarenko and T. Emonet for assistance with cell curvature analysis, H. Lam for plasmids, J. Wertz for technical help, and the members of the Jacobs-Wagner laboratory for critical reading of the manuscript.

This work was supported by the National Science Foundation GRFP (to M.T.C.), the Mustard Seed Foundation (to M.T.C.), a Howard Hughes Medical Institute predoctoral fellowship (to M.A.M.), NIH grants AI067548 (to G.J.J.) and GM076698 (to C.J.-W.), gifts to Caltech from the Gordon and Betty Moore Foundation and Agouron Institute, the Pew Scholars Program in the Biological Sciences, sponsored by the Pew Charitable Trust (to C.J.-W.), and the HEALTH-F3-2009-223431 DIVINOCELL collaborative project grant from the Commission of the European Communities (to W.V.). C.J.-W. and G.J.J. are Howard Hughes Medical Institute investigators.

REFERENCES

1. **Aaron, M., G. Charbon, H. Lam, H. Schwarz, W. Vollmer, and C. Jacobs-Wagner.** 2007. The tubulin homologue FtsZ contributes to cell elongation by guiding cell wall precursor synthesis in *Caulobacter crescentus*. Mol. Microbiol. **64:**938–952.
2. **Alyahya, S. A., R. Alexander, T. Costa, A. O. Henriques, T. Emonet, and C. Jacobs-Wagner.** 2009. RodZ, a component of the bacterial core morphogenic apparatus. Proc. Natl. Acad. Sci. U. S. A. **106:**1239–1244.
3. **Ausmees, N., J. R. Kuhn, and C. Jacobs-Wagner.** 2003. The bacterial cytoskeleton: an intermediate filament-like function in cell shape. Cell **115:** 705–713.
4. **Awram, P., and J. Smit.** 2001. Identification of lipopolysaccharide O antigen synthesis genes required for attachment of the S-layer of *Caulobacter crescentus*. Microbiology **147:**1451–1460.
5. **Bendezu, F. O., C. A. Hale, T. G. Bernhardt, and P. A. de Boer.** 2009. RodZ (YfgA) is required for proper assembly of the MreB actin cytoskeleton and cell shape in *E. coli*. EMBO J. **28:**193–204.
6. **Briegel, A., D. P. Dias, Z. Li, R. B. Jensen, A. S. Frangakis, and G. J. Jensen.** 2006. Multiple large filament bundles observed in *Caulobacter crescentus* by electron cryotomography. Mol. Microbiol. **62:**5–14.
7. **Cabeen, M. T., G. Charbon, W. Vollmer, P. Born, N. Ausmees, D. B. Weibel, and C. Jacobs-Wagner.** 2009. Bacterial cell curvature through mechanical control of cell growth. EMBO J. **28:**1208–1219.
8. **Cabeen, M. T., and C. Jacobs-Wagner.** 2005. Bacterial cell shape. Nat. Rev. Microbiol. **3:**601–610.
9. **Carballido-Lopez, R., and A. Formstone.** 2007. Shape determination in *Bacillus subtilis*. Curr. Opin. Microbiol. **10:**611–616.
10. **Charbon, G., M. T. Cabeen, and C. Jacobs-Wagner.** 2009. Bacterial intermediate filaments: in vivo assembly, organization, and dynamics of crescentin. Genes Dev. **23:**1131–1144.
11. **Chiang, S. L., and E. J. Rubin.** 2002. Construction of a mariner-based transposon for epitope-tagging and genomic targeting. Gene **296:**179–185.
12. **Cuthbertson, L., J. Powers, and C. Whitfield.** 2005. The C-terminal domain of the nucleotide-binding domain protein Wzt determines substrate specificity in the ATP-binding cassette transporter for the lipopolysaccharide O-antigens in *Escherichia coli* serotypes O8 and O9a. J. Biol. Chem. **280:** 30310–30319.
13. **D'Elia, M. A., M. P. Pereira, Y. S. Chung, W. Zhao, A. Chau, T. J. Kenney, M. C. Sulavik, T. A. Black, and E. D. Brown.** 2006. Lesions in teichoic acid biosynthesis in *Staphylococcus aureus* lead to a lethal gain of function in the otherwise dispensable pathway. J. Bacteriol. **188:**4183–4189.
14. **de Lorenzo, V., M. Herrero, U. Jakubzik, and K. N. Timmis.** 1990. Mini-Tn*5* transposon derivatives for insertion mutagenesis, promoter probing, and chromosomal insertion of cloned DNA in gram-negative eubacteria. J. Bacteriol. **172:**6568–6572.
15. **Edwards, P., and J. Smit.** 1991. A transducing bacteriophage for *Caulobacter crescentus* uses the paracrystalline surface layer protein as a receptor. J. Bacteriol. **173:**5568–5572.
16. **Ely, B.** 1991. Genetics of *Caulobacter crescentus*. Methods Enzymol. **204:**372–384.
17. **Evinger, M., and N. Agabian.** 1977. Envelope-associated nucleoid from *Caulobacter crescentus* stalked and swarmer cells. J. Bacteriol. **132:**294–301.
18. **Gitai, Z., N. Dye, and L. Shapiro.** 2004. An actin-like gene can determine cell polarity in bacteria. Proc. Natl. Acad. Sci. U. S. A. **101:**8643–8648.
19. **Glauner, B.** 1988. Separation and quantification of muropeptides with high-performance liquid chromatography. Anal. Biochem. **172:**451–464.
20. **Keen, N. T., S. Tamaki, D. Kobayashi, and D. Trollinger.** 1988. Improved broad-host-range plasmids for DNA cloning in gram-negative bacteria. Gene **70:**191–197.
21. **Lam, H., W. B. Schofield, and C. Jacobs-Wagner.** 2006. A landmark protein essential for establishing and perpetuating the polarity of a bacterial cell. Cell **124:**1011–1023.
22. **Matroule, J. Y., H. Lam, D. T. Burnette, and C. Jacobs-Wagner.** 2004. Cytokinesis monitoring during development; rapid pole-to-pole shuttling of a signaling protein by localized kinase and phosphatase in *Caulobacter*. Cell **118:**579–590.
23. **Osborn, M. J., and L. Rothfield.** 2007. Cell shape determination in *Escherichia coli*. Curr. Opin. Microbiol. **10:**606–610.
24. **Raetz, C. R., C. M. Reynolds, M. S. Trent, and R. E. Bishop.** 2007. Lipid A modification systems in gram-negative bacteria. Annu. Rev. Biochem. **76:** 295–329.
25. **Raetz, C. R., and C. Whitfield.** 2002. Lipopolysaccharide endotoxins. Annu. Rev. Biochem. **71:**635–700.
26. **Ravenscroft, N., S. G. Walker, G. G. Dutton, and J. Smit.** 1991. Identification, isolation, and structural studies of extracellular polysaccharides produced by *Caulobacter crescentus*. J. Bacteriol. **173:**5677–5684.
27. **Ravenscroft, N., S. G. Walker, G. G. Dutton, and J. Smith.** 1992. Identification, isolation, and structural studies of the outer membrane lipopolysaccharide of *Caulobacter crescentus*. J. Bacteriol. **174:**7595–7605.
28. **Roberts, R. C., C. Toochinda, M. Avedissian, R. L. Baldini, S. L. Gomes, and L. Shapiro.** 1996. Identification of a *Caulobacter crescentus* operon encoding hrcA, involved in negatively regulating heat-inducible transcription, and the chaperone gene grpE. J. Bacteriol. **178:**1829–1841.
29. **Shiomi, D., M. Sakai, and H. Niki.** 2008. Determination of bacterial rod shape by a novel cytoskeletal membrane protein. EMBO J. **27:**3081–3091.
30. **Simon, R., U. Prieffer, and A. Puhler.** 1983. A broad host range mobilization system for in vivo genetic engineering: transposon mutagenesis in gram-negative bacteria. Biotechnology (NY) **1:**784–790.
31. **Smit, J., and N. Agabian.** 1984. Cloning of the major protein of the *Caulobacter crescentus* periodic surface layer: detection and characterization of the cloned peptide by protein expression assays. J. Bacteriol. **160:**1137–1145.
32. **Smit, J., D. A. Grano, R. M. Glaeser, and N. Agabian.** 1981. Periodic surface array in *Caulobacter crescentus*: fine structure and chemical analysis. J. Bacteriol. **146:**1135–1150.
33. **Soding, J., A. Biegert, and A. N. Lupas.** 2005. The HHpred interactive server for protein homology detection and structure prediction. Nucleic Acids Res. **33:**W244–W248.
34. **Takacs, C. N., S. Poggio, G. Charbon, M. Pucheault, W. Vollmer, and C. Jacobs-Wagner.** 2009. MreB drives de novo rod morphogenesis in *Caulobacter crescentus* via remodeling of the cell wall. J. Bacteriol. **192:**1671–1684.
35. **Tatar, L. D., C. L. Marolda, A. N. Polischuk, D. van Leeuwen, and M. A. Valvano.** 2007. An *Escherichia coli* undecaprenyl-pyrophosphate phosphatase implicated in undecaprenyl phosphate recycling. Microbiology **153:** 2518–2529.
36. **Tsai, C. M., and C. E. Frasch.** 1982. A sensitive silver stain for detecting lipopolysaccharides in polyacrylamide gels. Anal. Biochem. **119:**115–119.
37. **Walker, S. G., D. N. Karunaratne, N. Ravenscroft, and J. Smit.** 1994. Characterization of mutants of *Caulobacter crescentus* defective in surface attachment of the paracrystalline surface layer. J. Bacteriol. **176:**6312–6323.
38. **Walker, S. G., S. H. Smith, and J. Smit.** 1992. Isolation and comparison of the paracrystalline surface layer proteins of freshwater caulobacters. J. Bacteriol. **174:**1783–1792.
39. **Wang, Y., B. D. Jones, and Y. V. Brun.** 2001. A set of ftsZ mutants blocked at different stages of cell division in *Caulobacter*. Mol. Microbiol. **40:**347–360.
40. **Whitfield, C.** 2006. Biosynthesis and assembly of capsular polysaccharides in *Escherichia coli*. Annu. Rev. Biochem. **75:**39–68.
41. **Wolgemuth, C. W., N. W. Charon, S. F. Goldstein, and R. E. Goldstein.** 2006. The flagellar cytoskeleton of the spirochetes. J. Mol. Microbiol. Biotechnol. **11:**221–227.